

Intergrain necking and the reversal of magnetization of fine, highly acicular ferromagnetic skeleton particles

K. OHSHIMA

Computational Science Department, Performance Materials Research and Development Center, Research and Development Division, Mitsui Chemicals Inc., 1190, Kasama-Cho, Sakae-Ku, Yokohama City, 247 Japan
E-mail: ohshima@mitsui-chem.co.jp

In this paper the relationship between the reversal of magnetization and the morphology of very fine, iron-based and highly acicular particles used in high-density magnetic recording media is investigated. The iron-based particle referred here is of a skeleton type, which consists of a very fine granular material; the so-called "grain". The grain belongs to the bcc phase and its size ranges between about 100 to 300 Å depending on usage. Therefore the grain can be treated as a single domain particle. As the morphology of the skeleton particle prepared for 8 m/m video-recording media is mainly determined by the grain size and the intergrain necking, the effects on the coercivity were studied. The magnetization reversal of a long "chain-of-spheres" which are in contact with each other over a finite area was investigated to determine the quantitative relationship with "intergrain necking" of the skeleton particles when a type of "exchange anisotropy", which is proportional to the contact area between two adjacent unit spheres, is introduced into the chain. The symmetric fanning mode is preferential in increasing the intergrain necking. The introduction of the exchange anisotropy can result in decrease in the coercivity with increasing intergrain necking, this quantitatively reproduces the experimental behavior observed for very fine, highly acicular skeleton particles of α -Fe. On the other hand, no essential change in the behavior of the angular variation of the coercivity is induced even if exchange anisotropy is introduced into the chain. Finally, under the present scheme, it has been discussed as to how to interpret the experimentally-found dependence of coercivity on grain size, where a possibility to introduce an influence of the unit-sphere size on the characteristic constant of the exchange anisotropy is suggested.

© 2001 Kluwer Academic Publishers

1. Introduction

In this paper, we study the experimental and theoretical effects of the particle morphology of very fine, acicular particles of α -Fe, which are prepared for 8 m/m video-recording media, on magnetization reversal. As the particle morphology is very complicated, we present a short review before describing the experimentation.

A conventional method for synthesizing the pigment of the very fine, acicular particles of α -Fe is as follows. Usually, submicrometer-order acicular particles of goethite with an aspect ratio of about 10 are selected as the starting material, this is followed by dehydration, reduction and/or oxidation under a selected chemical atmosphere. Due to a contact reaction under the gaseous phase at relatively higher temperatures, agents to help avoid interparticle sintering are introduced onto the particle surface of the goethite to keep the acicularity of the geometrical shape.

Although the starting material goethite, is a single crystal that crystallographically belongs to the orthorhombic system, the synthesized oxide or metal particles are of a very complicated nature. As is shown in Fig. 1, the α -Fe particles are not of the single crystal type, but of the so-called *skeleton type*, this shows up as a mosaic structure consisting of crystal grains with size of the order of 10^2 Å.

It is very important to establish the quantitative relationship between the pigment characteristics and the magnetization reversal properties for high-density audio/video recording-use iron-based fine acicular particles. Within this field, it is possible to find at least *five* "to-be-solved-problems". *The first problem* is to develop a morphological characterization of the skeleton particle of α -Fe. In particular, crystallographic identification with respect to the stacking mode of the grains in the particle is important. *The second problem* is to systematically investigate the experimental relationship



Figure 1 A typical transmission electron microscope image showing the morphology of very fine, acicular particles of α -Fe prepared for 8 m/m video recording media. The particle is of a skeleton type and not the single crystal type. The image shows a mosaic structure consisting of grains with size in of order of 100 Å. The grain crystallographically belongs to the bcc phase and its shape is that of a rhombic dodecahedron. Sometimes, pores are included in the particles themselves. Furthermore, the particles easily form local aggregates which are called “multiple” or “bundle”.

between the skeleton particle morphology and the magnetization reversal properties. In particular, the quantitative effects of the grain size, the necking between the grains and the volume content of the pores on the reversal of magnetization are important. *The third problem* is to geometrically model the skeleton-particle morphology. In this model, it should be possible to represent the pores of the skeleton particle. *The fourth problem* is to simulate the reversal of magnetization using this morphological model, from this model we need to be able to determine how the particle morphology affects the reversal of the magnetization. Finally, the author has a *fifth problem*, which simulates the reversal of magnetization for the interacting skeleton particles. In this simulation, we need to find the most important factor affecting the mechanism of magnetization reversal in the interacting system.


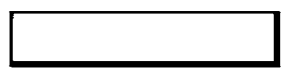
Apart from a theoretical understanding of the experimentally-found effects of the grain size and intergrain necking on the coercivity (H_c), the possible experimental and theoretical solutions for the five given problems have been determined by the author [1–7]:

For the first problem, the author has found that

(1) The particle is of a *skeleton* type consisting of bcc phase crystal grains, or so-called crystallites whose size ranges from approximately 100 to 300 Å depending on the preparation process used.

(2) There are, at least, *two* types of grain stacking modes (Table I and Fig. 2a and b). In the first type of stacking mode, one of the principal axes of the bcc phase, aligns with the long axis of the acicular particle. In the second type, one of the directions normal to {110}-planes aligns along the long axis of the particle.

TABLE I Two side-view images found for the particle morphology of the acicular skeleton type of α -Fe^a and their possible crystallographical orientation with the grains^b [2, 3]

	apparent Side-View
Type -D	
Type -S	

^aAfter much experience in observing the morphological shape of the acicular skeleton particles of α -Fe, it is our understanding that the particle morphology can be classified into two types, *type-D*, where the crystal grains are connected in a planar-zigzag and *type-S*, where the grains form a linear-like chain. In the cases, where (1) the goethite particles of the starting materials are of the “fatter” type whose diameter is larger than about 200 Å, or (2) the anti-sintering agents introduced onto the particles to ensure that the acicularity of the shape consist dominantly of Si-containing glassy compounds, or (3) the reduction is carried out under a water-free hydrogen atmosphere, or (4) the binding between the grains is weak, *type-D* particles are usually produced. In contrast, it is empirically found that, in the cases where (1) the goethite particles are of the “slender” type with a diameter smaller than about 200 Å, or (2) the anti-sintering agents introduced onto the particles consist dominantly of B-containing glassy compounds, or (3) the reduction is carried out at relatively higher temperatures, or (4) the binding between the grains is strong, *type-S* particles are usually formed. This table was reused by kind permission of the IEEE.

^bFor *type-D* particles, [001] is in parallel with the major long axis, whereas in the *type-S*, [110] with it.

The existence of both types is being directly proven by the microscopic electron diffraction technique.

(3) In the acicular skeleton particle, microscopic pores exist whose size is of the same order (or smaller) than that of the crystal grains. The presence of the pores could be due to intergrain misfitting.

(4) The acicular particles could very easily form *local aggregates* which are termed the “multiple” or the “bundle”.

For the second problem, it was found that

(5) It is possible to experimentally describe the skeleton-particle morphology in terms of *the grain size*, *intergrain necking* and *the intraparticle pores*; these morphological parameters strongly affected the value of H_c . In particular, the effect of the intraparticle pores on the value of H_c can be quantitatively explained by our model theory described in the following point, (6).

The third and fourth problems were solved as follows:

(6) The “*chain-of-spheres*” *fanning model* originally proposed by Jacobs and Bean [8] can be used as a starting model which is applicable to acicular skeleton type particles of α -Fe. By the introduction of the contact

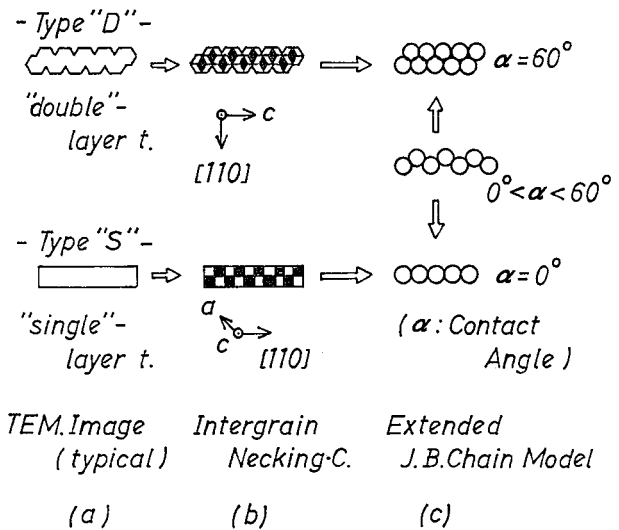


Figure 2 Morphological modeling of the acicular skeleton type particle of α -Fe. To investigate the relationship between the morphology of the skeleton type particles and the reversal of magnetization, the author considered that the “chain-of-spheres” as originally proposed by Jacobs and Bean [8] could be a starting morphological model. This model represents a linear chain consisting of n spheres with the diameter, a , all point-contacting each other (this chain is termed the Jacobs-Bean’s chain, or JB chain or JBC). As is well known, if each sphere can be assumed to be a dipole unit with the moment, μ , the reversal of magnetization of a single JBC can be physically determined by the dipole-dipole type of the static magnetic interaction among the spheres under a given external magnetic field. The author has extended this JBC by the introduction of a contact angle, α , between two adjacent, nearest neighbors. A contact angle of $\alpha = 0^\circ$ means that the chain is of an extended type, that is the JBC. A chain where $\alpha = 60^\circ$, corresponds to a doubled chain type and when α ranges from 0° to 60° , this provides a planar-zigzag chain. Since the chain with a non-zero α bends and snakes locally, we call this type of extension to the JBC the snaked JBC or SJBC. It was possible to relate the SJBC with an α value of 0° and 60° to the skeleton particle of *type-S* and *type-D* respectively, as described in Table I. It was assumed that the morphological characteristics of the SJBC can be given by two parameters, (n , and α), and also that the intraparticle pores can be mathematically estimated by an introduction of the unit spheres without the dipole moment. This figure has been reused by kind permission of the IEEE.

angle between two adjacent spheres in the chain, it becomes possible to correlate the chain-of-spheres with the various types of experimentally observed particle morphologies (Fig. 2c).

(7) The physically possible *dipole conformation* is strongly dependent on the particle morphology; the symmetric fanning of the dimer repeating unit is most realizable when in the extended and/or planar-zigzag type of chain, represented by the contact angles of zero and/or a finite value less than 60° , respectively. A modified fanning of the tetramer unit would be most likely in the doubled chain, which is given by a contact angle of 60° .

Finally, for the fifth problem, extensive numerical simulation has been carried out to obtain following results:

(8) It has been possible to extend the model theory described in (6) to an interacting chain system forming an infinite regularly spaced lattice.

(9) Application of this theory shows that the formation of local aggregates as described in (4) results in a very large lowering of H_c . Furthermore, this type of application leads to a quantitative investigation of the

packing fraction dependence of H_c as observed in the highly orientated sheet material made from the pigment of α -Fe particles described in (1–4). It is predicted that in extremely high packing states, a “chain-of-particles” will be formed.

(10) It is quantitatively possible to use our method to investigate the effect of the interparticle interaction on the angular variation of H_c as only the magnetostatic lateral interchain interaction can affect the angular variation of H_c . Furthermore, it is strongly suggested that a local aggregate of the type of so-called “multiple” is unavoidably generated in a realistic system; this leads to the angular variation of H_c with a complex and deviated behavior from the “coherent” particles.

In this paper, “not-yet-solved problems”, which are related to the theoretical interpretation regarding the effects of grain size and the intergrain necking on H_c in (5) are investigated within the framework of the long “chain-of-spheres”, which contact each other over a finite area. A theoretical approach to this problem was first carried out by Ishii and Sato [9] by the introduction of a model system consisting of two interacting “dipole spheres” contacting each other over a finite area. Although they have not used the “necking” or “sintering” concepts, increasing the contact area in their model corresponds to an increase in the intersphere “necking” or “sintering” in the sense used in this paper (hereafter, only the term “necking” will be used to avoid unnecessary confusion). It was found that, (a) there was an essential enhancement of the symmetric fanning mechanism in the same way as in Jacobs-Bean’s treatment [8] and (b) that the values and the angular variations of the nucleation field, H_n and H_c are influenced by introducing a finite contact area. However, the “pure” dependence of H_n , H_c and their angular variations on the intersphere necking was not so clear because the aspect ratio of the chain “simultaneously” and rapidly decreases when the contact area increases in their chain.

It is now well known that the fine acicular particles used in the high density magnetic recording media of the present day are mainly of the type of (Co-modified) γ -Fe₂O₃, CrO₂ and/or α -Fe with a high aspect ratio of about 8 or 10, or sometimes up to 15. Therefore, the extension of Ishii-Sato’s treatment to geometrically reflect the acicularity of the realistic particle would be very important, if we would like to know the relationship between the morphology and the magnetic properties of a fine, acicular particle.

2. Theoretical treatment

According to several of our previously published papers regarding the relationship between the morphology and the magnetic properties of a fine, acicular skeleton particle for 8 m/m video-recording use [1–7], it has basically been shown that this type of particle can be geometrically represented by the “chain-of-spheres” which was originally introduced by Jacobs and Bean [8] known as JBC (Jacobs-Bean’s Chain). In a JBC, each unit-sphere is defined such that, (a) it contacts with another sphere at a point such that they form a straight, linear chain and (b), that it has a unit-dipole moment which inter-

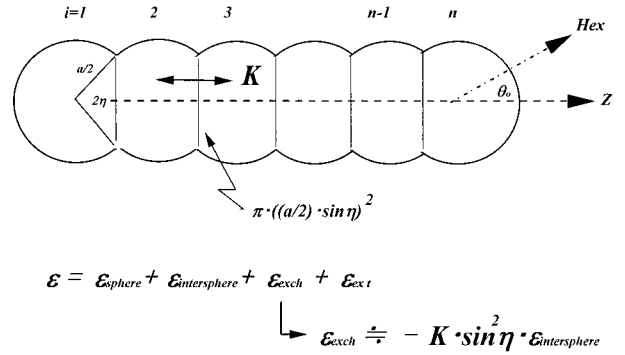


Figure 3 Schematic illustration of an extended Ishii-Sato’s chain where the component spheres with the dipole moment μ , contact each other over a finite area [9]. η is the “necking” or “sintering” angle between the spheres and a characteristic in the scheme. The chain where $\eta = 0^\circ$ corresponds to the Jacobs-Bean’s chain-of-spheres. Note that the number of the spheres, n , in the original Ishii-Sato’s chain is 2. Therefore, in the case of the extended chain type considered here, a new magnetic interaction can be found between the neighboring spheres. In this chain, because of the finite contact area between the dipole spheres, there should be a type of “exchange anisotropy” through the contact area. To introduce this type of exchange anisotropy into the theory, it was assumed that the exchange interaction is proportional to the contact area. For further details, refer to the main text.

acts with others through a long-ranged interaction of the dipole-dipole type.

In order to theoretically estimate the effect of intersphere necking on the magnetization reversal, an extension of Ishii-Sato’s treatment [9] was tried (hereafter, referred to as the modified JBC as ISC or IS chain, standing for “Ishii-Sato’s Chain”). Fig. 3 shows an extended ISC, where the original type consists of two spheres. The original chain is now extended to a type with a sphere number of (at least) 8 or 10, and takes the morphology of the realistic fine acicular skeleton particles into account.*[†] This extended Ishii-Sato’s chain is

* The author should comment on two papers by Ishii and Sato. After writing the first manuscript of this paper (End of Dec. 1996), it was found (Jan. 10th 1997) that the two papers by Y. Ishii and M. Sato [10, 11], reference the original discussions regarding the “ISChain” with two spheres (Ref. 9). Ref. [10] was concerning the “magnetic behaviors of elongated-single-domain particles by chain-of-spheres model”, while Ref. [11] concerned the “rotational hysteresis of elongated-single-domain particles by chain-of-spheres model”. In both of these papers, a long-sized chain-of-spheres contacting each other over a finite area had been investigated. Our method described in Appendix C, which mathematically shows how to extend the ISC with two spheres is essentially the same with their treatment. In particular in Ref. [10], they briefly discussed an effect of the exchange interaction between the spheres, where their exchange interaction is also proportional to the contacting area, in the same way as we have assumed in this paper.

However, their results do not contain (a) the quantitative effect of the anisotropy constant which estimates the “strength” of the exchange interaction and (b) the application of the model theory to the experimental behavior with respect to the dependence of H_c and its angular variation on the intergrain necking and grain size. In particular, because the surface structure of the industrially prepared fine acicular skeleton particles of α -Fe is not “pure” [12], then the exchange interaction occurring between the spheres must be very complicated. Therefore, a quantitative study of the effect of the anisotropy constant is necessary. Although the author cannot find any “priority” for the model which treats the long-sized ISC with an exchange anisotropy, it was believed to be worthwhile to apply this model to the experiments in order to study the physical meaning of the size-dependence of H_c .

[†] The complicated properties of the particle surface of α -Fe was reported in the author’s most recent experimental paper, “On the Reactivity of Organic Solvents on the Particle Surface of Metal Pigment” [12].

characterized by the “necking” angle, η , and the number of the spheres, n . Mathematical formulation of this type of magnetization reversal of the ISC is basically straightforward and therefore, only the simplified description of our method of how to treat a long-sized ISC is presented here. Because, in the long-sized ISC, estimation of several new types of sphere interactions are necessary, Appendix A precisely describes the mathematical reformulation for the single long-sized ISC under an external magnetic field. The geometrical characterization of the ISC is given in Appendix B.

It is convenient to represent the total energy density, ε_{tot} , of a single long-sized ISC under an external magnetic field as a sum of three parts:

$$\varepsilon_{\text{tot}} = \varepsilon_{\text{sphere}} + \varepsilon_{\text{intersphere}} + \varepsilon_{\text{ext}}. \quad (1)$$

The third term to the right-hand side of Equation 1, ε_{ext} , represents the interaction between the dipole on each sphere and an external field. Therefore, only a description of the first and second terms is necessary. The first term, $\varepsilon_{\text{sphere}}$, represents the total self-energy of the dipole distributed on each sphere. It is represented by a linear combination:

$$\varepsilon_{\text{sphere}} = \sum_{i=1}^n \varepsilon_{\text{sphere}}(i), \quad (2)$$

where each sphere’s contribution, $\varepsilon_{\text{sphere}}(i)$ for $i = 1, 2, \dots, n$, can be given by

$$\varepsilon_{\text{sphere}}(i) = C \cdot (\sin^2 \theta_i \cdot P_{s,i} + \cos^2 \theta_i \cdot Q_{s,i}). \quad (3)$$

C , in Equation 3 is a factor which is dependent on sphere size, the dipole moment of a sphere and the effective volume occupied by the chain and contains a constant that is dependent on the unit system used. θ_i is the polar angle of the dipole moment on the i -th sphere. $P_{s,i}$ and $Q_{s,i}$ are characteristic parameters which are represented by a double integral whose integrand includes the complete elliptic integral of the second and first kind, respectively (for explicit representations, see, Equations A.2d and e in Appendix A). All $\{P_{s,i}\}$ and $\{Q_{s,i}\}$ for $i = 1, 2, \dots, n$ can be numerically estimated as a function of the intersphere necking angle, η (the numerical values for the ISC with $n = 10$ are tabulated in Appendix C). Note that $\{P_{s,i}\}$ and $\{Q_{s,i}\}$ for $i = 2, 3, \dots, n - 1$ ($n \geq 3$), as for $P_{s,2}$ and $Q_{s,2}$ for ISC with $n = 3$, are interaction parameters of the *new* type which do not appear in Ishii-Sato’s original treatment.

The second term of the right-hand side of Equation 1, $\varepsilon_{\text{intersphere}}$, is the contribution from the dipole-dipole interaction among n -spheres and can be represented by:

$$\varepsilon_{\text{intersphere}} = \sum_{i=1}^n \sum_{j=i+1}^n \varepsilon_{\text{intersphere}}(i, j). \quad (4)$$

In Equation 4, the interaction term between i -th and j -th sphere, $\varepsilon_{\text{intersphere}}(i, j)$, is given by

$$\varepsilon_{\text{intersphere}}(i, j) = C \cdot \{\sin \theta_i \cdot \sin \theta_j \cdot \cos(\phi_i - \phi_j) \cdot P_{m,ij} + \cos \theta_i \cdot \cos \theta_j \cdot Q_{m,ij}\}, \quad (5)$$

where $P_{m,ij}$ and $Q_{m,ij}$ are, as $P_{s,i}$ and $Q_{s,i}$, two characteristic parameters which are represented by the double integral whose integrand includes the complete elliptic integral of the second and first kind respectively (for the explicit representations, see, Equations A.3c and d in Appendix A). All $\{P_{m,ij}\}$ and $\{Q_{m,ij}\}$ for $(i, j) = 1, 2, \dots, n$ can be numerically estimated as a function of η (the numerical values for ISC with $n = 10$ are tabulated in Appendix C). Again note that $\{P_{m,ij}\}$ and $\{Q_{m,ij}\}$ for $(i, j) = 1, 2, 3, \dots, n$ with $|i - j| \geq 1$ ($n \geq 3$), as for $P_{m,23}$ and $Q_{m,23}$ for ISC with $n = 3$, are interaction parameters of the *new* type which do not appear in Ishii-Sato’s original treatment. Detailed treatment of Equation 1 to simulate the magnetization reversal process under the parallel and symmetric fanning modes is given in Appendix A.

In the ISC, because of the finite contact between dipole spheres, a kind of “exchange anisotropy” should exist through the contact area. Therefore, another term is necessary in the energy-density expression, Equation 1. To introduce this type of the exchange anisotropy into the theory, it was assumed that the energy of the exchange interaction between two nearest neighboring spheres, $\varepsilon_{\text{exch}}(i, j = i + 1)$, is *proportional* to the contact area ($\pi a^2 \sin^2 \eta / 4$ where a is the diameter of the sphere) and the energy due to the dipole-dipole interaction between two nearest neighboring spheres ($\varepsilon_{\text{intersphere}}(i, j = i + 1)$ in Equation 1). Then, the exchange interaction energy can be estimated formally as:

$$\varepsilon_{\text{exch}}(i, j = i + 1) = -K \cdot \sin^2 \eta \cdot \varepsilon_{\text{intersphere}}(i, j = i + 1) \quad \text{for } i = 1, 2, 3, \dots, n - 1, \quad (6)$$

where K is a dimensionless constant representing the effective “exchange anisotropy” [13]. Furthermore, as is shown in Fig. 4 and given in Appendix C, the values of $P_{m,ij}$ and $Q_{m,ij}$ with $j > i + 1$ for $i = 1, 2, 3, \dots, n - 2$ tend to zero rapidly, Equation 6 can be approximated within a negligible numerical errors by the following equation:

$$\varepsilon_{\text{exch}} = -K \cdot \sin^2 \eta \cdot \varepsilon_{\text{intersphere}}, \quad (7)$$

where $\varepsilon_{\text{exch}}$ is the exchange energy between the neighboring spheres. Since the total dipole-dipole interaction including the exchange term apparently decreases by the factor, $1 - K \cdot \sin^2 \eta$, in this approximation therefore, the total energy density, ε_{tot} , of a single long-sized Ishii-Sato’s chain under an external magnetic field is modified as follows instead of as in Equation 1:

$$\varepsilon_{\text{tot}} = \varepsilon_{\text{sphere}} + (1 - K \cdot \sin^2 \eta) \varepsilon_{\text{intersphere}} + \varepsilon_{\text{ext}}. \quad (8)$$

As shown in Appendix A, the reversal of the magnetization of the single long-sized ISC can be quantitatively estimated by using the characteristic parameters, $\{P_s, Q_s\}$ from the “on-sphere” dipole-dipole interaction and $\{P_m, Q_m\}$ from the “inter-sphere” dipole-dipole interaction. These double integrations were numerically calculated by using a Vector Processor,

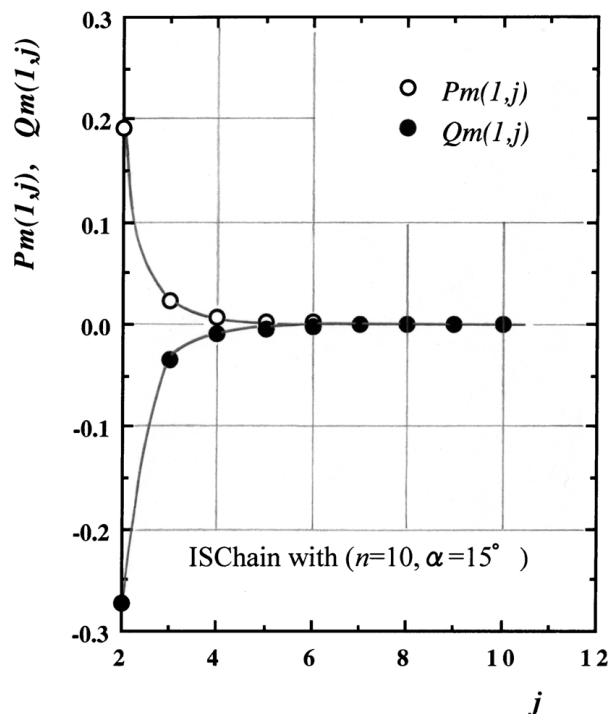


Figure 4 Characteristic parameters, $P_m(i=1, j)$ and $Q_m(i=1, j)$ as a function of j for an ISC where $n=10$ and $\eta=15^\circ$. The values of $P_m(i, j)$ and $Q_m(i, j)$ are essentially finite between the nearest ($j=i+1$) and next nearest ($j=i+2$) neighbors only.

VP-2100/10 of Fujitsu Ltd. The numerical accuracy of the computation method for these integrations was independently cross-checked using Convex-3210/50 in the form of another type of algorithm for the computations. Appendix C provides the numerical values of $\{P_s, Q_s\}$ and $\{P_m, Q_m\}$ for the ISC with $n=10$. It was confirmed that in the case with $n=2$, this completely coincides with the Ishii-Sato's result [9]. From the numerical estimations on these characteristic parameters for an assumed value of (n, η) , the values of H_n and H_c and their angular variations were obtained numerically, where two types of the dipole conformation, the symmetric fanning and parallel rotation mechanism in the sense of Jacobs-Bean [8], were assumed.

3. Computation results

3.1. H_n and H_c as a function of θ_0 and η

For the symmetric fanning and parallel rotation modes of the dipole conformation in the ISC with $n=10$, the behaviors of H_n and H_c are shown as a function of the aligned angle of the chain to an external field, θ_0 , and the necking angle, η , in Fig. 5a and b.

From these figures, it can be seen that H_n , H_c , and their angular variations depend on the intersphere necking. These behaviors are grossly similar to those for the ISC where $n=2$, except that the enhancement region of the symmetric fanning mode is widely extended in the aligned and necking angles. One of the reasons for this is presumably to keep the acicularity of the long-sized ISC even when the intersphere necking increases.

The calculations were repeated for the ISC when $n=3, 4$ and 5 , and a multi-regression analysis was then carried out to obtain the "pure" effect of the intersphere necking, as defined in Appendix B, on the reversal of the

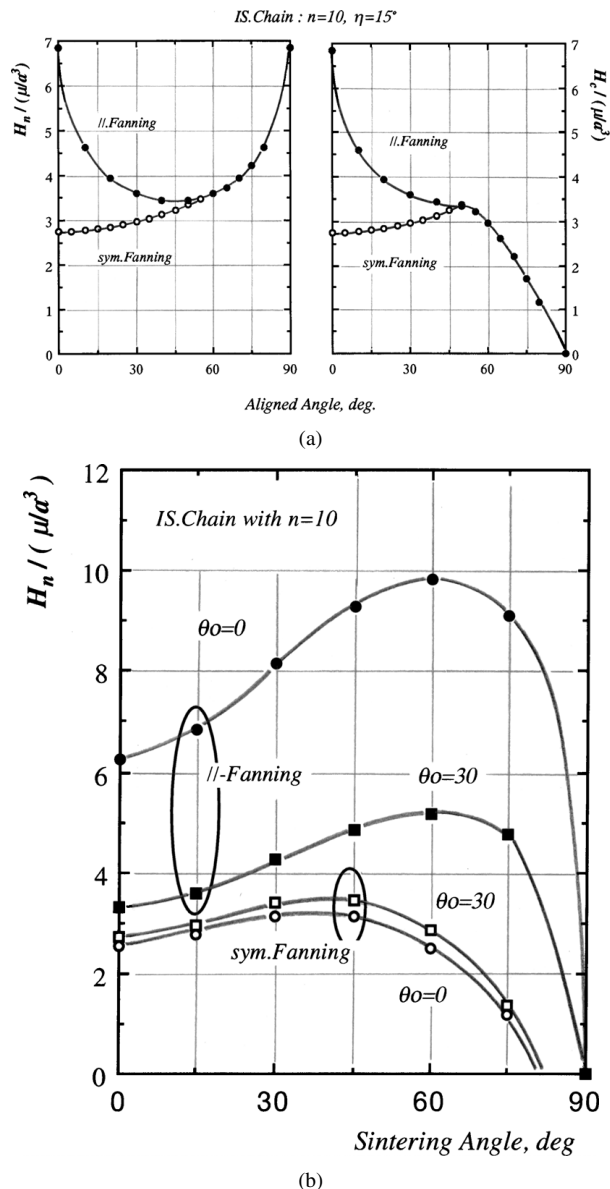


Figure 5 (a) The (calculated) angular variation of the nucleation field, H_n , and coercivity, H_c , for an ISC where the number of the spheres $n=10$ and the necking angle $\eta=15^\circ$. Both the symmetric and parallel fanning modes are taken into account. (b) Nucleation field plotted against necking angle for an ISC where $n=10$. Two cases of the aligned angle are considered ($\eta=0$ and 30°). Both the symmetric and parallel fanning modes are taken into account.

magnetization. For full results see Appendix D. Fig. 6 shows one of the results obtained, where the aligned ISC with the effective aspect ratio of 10 in the symmetric fanning mode is taken into account; here, H_c increases by less than 0.5 with the intersphere necking, p , and then decreases with p . As far as the author is aware, this is the *first* theoretical prediction regarding the "pure" dependence of H_c on intersphere necking. However, as will be seen, this p -dependence of H_c does *not* coincide with the experimental trend due to the neglect of the exchange anisotropy mentioned previously.

3.2. Effect of "exchange anisotropy"

The effect of the exchange anisotropy acting through the contact area on the magnetization reversal was next estimated, one of the results obtained is shown in Fig. 7a. By increasing the exchange anisotropy, K ,

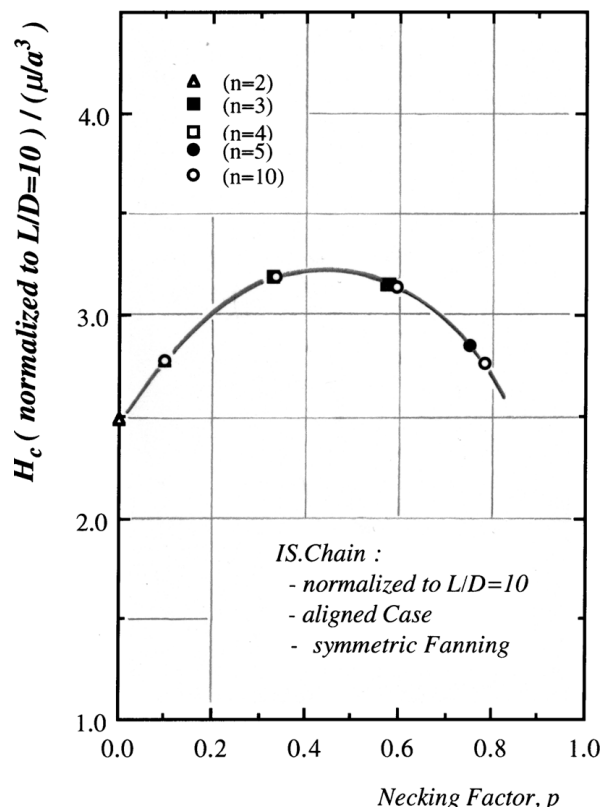


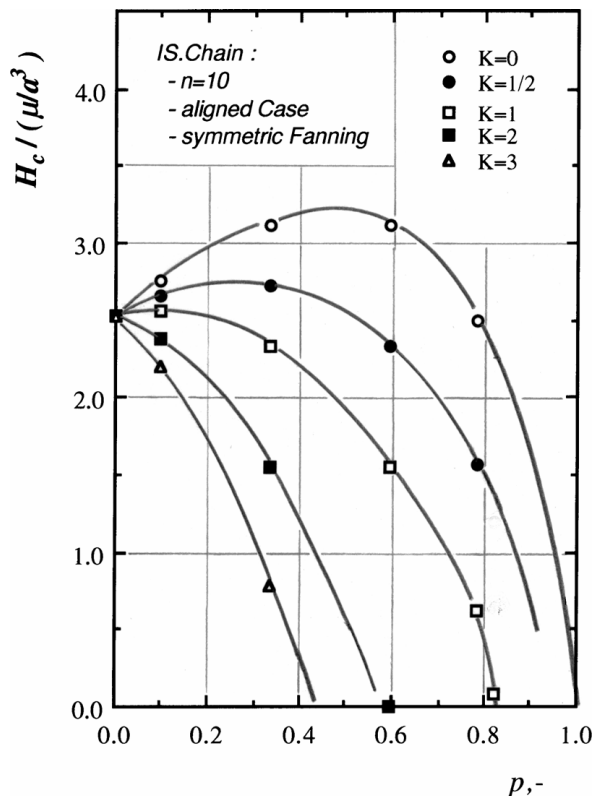
Figure 6 Dependence of H_c on the necking factor, p , for an ISC in the symmetric fanning mode. Note that the ISC is normalized to $L/D = 10$.

a drastic change in the dependence of H_c on the intersphere necking is induced, the larger value of K provides a smoothed behavior of H_c with the intersphere necking, p . In particular, K values larger than about 1 result in H_c decreasing with p .

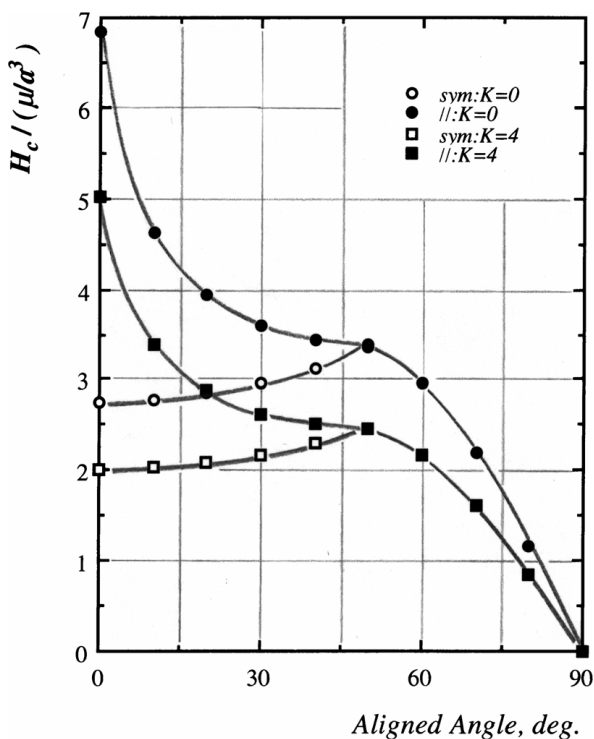
On the other hand, Fig. 7b shows that there is “no” essential change in the angular variation of H_c even when the large exchange anisotropy is introduced (note here that although in the parallel fanning mode there is no exchange interaction acting between the spheres, Fig. 7b formally shows the effects of K on the angular variation of H_c in the parallel fanning mode in comparison with the case in the symmetric fanning mode). This is very important when the theoretical approach is tried under the chain-of-spheres fanning mode to explain the angular variation of H_c . This is apparently similar to that of the infinitely long rod-shaped particle under the *curling* mode of the incoherent scheme of the reversal of magnetization [14–17].

4. Comparisons with experiments

45 different species of skeleton particles of α -Fe with an aspect ratio of about 10 were synthesized using three different chemical modifications of the same starting material (goethite particle, α -FeOOH) with five different calcination temperatures and three different reduction temperatures (see Table II). The skeleton particle morphology could be characterized by the specific surface area, the grain size and the particle density or the degree of intergrain necking [5]. The “pure” effect of the intergrain necking on H_c was obtained as shown in Fig. 8a from (a) a multi-regression analysis of the observed H_c with the specific surface area, the grain size



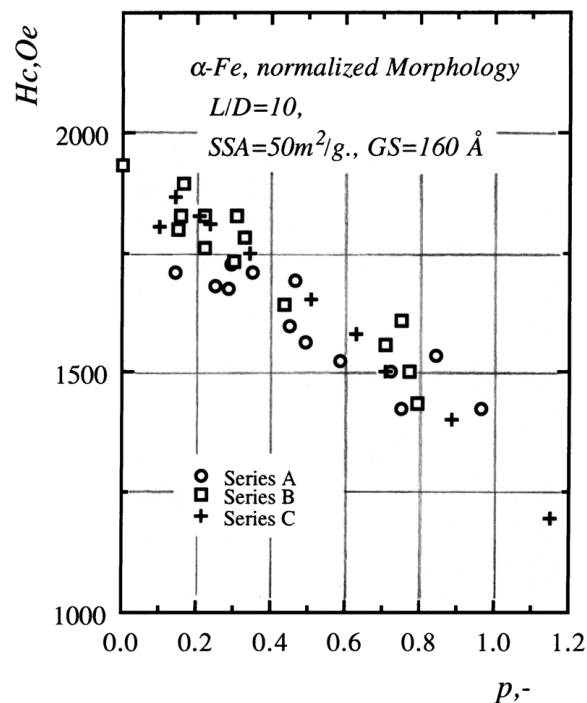
(a)



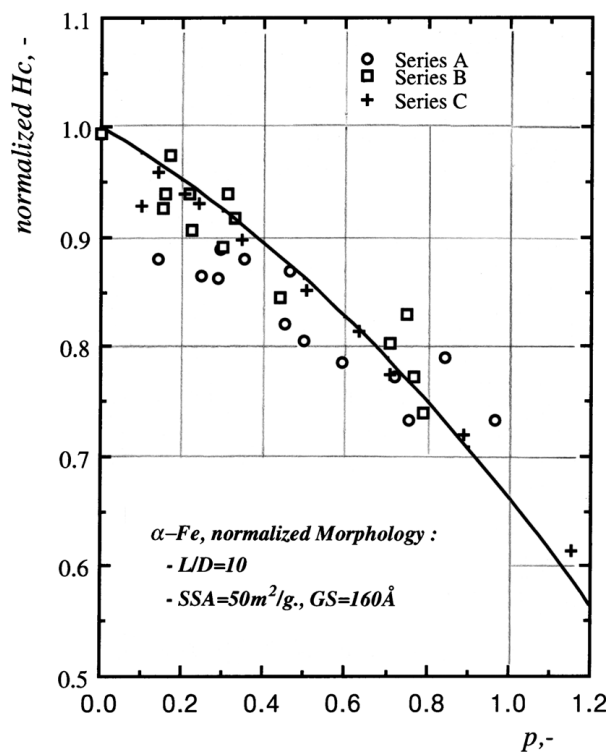
(b)

Figure 7 (a) The influence of “exchange anisotropy” on the dependence of H_c on the necking factor for an ISC where $n = 10$ in the symmetric fanning mode. (b) Effect of “exchange anisotropy” on the angular variation of H_c for an ISC where $n = 10$ and $\eta = 15^\circ$. Note that in the case of the parallel fanning mode, no exchange interaction occurs between the spheres. Therefore, only the apparent behavior for this fanning mode is shown here.

and the particle density estimated experimentally and by (b) assuming a “normalized” morphology which is characterized by a specific surface area of $50 \text{ m}^2/\text{g}$ and a grain size of 160 \AA , this being typical for the particles



(a)



(b)

Figure 8 (a) The experimental dependence of H_c on the necking factor, p , for very fine, highly acicular skeleton-particles of α -Fe. (b) Explanation of the p -dependence of H_c as observed for α -Fe with a normalized morphology by the present model with the exchange anisotropy constant, $K = 3.26$. See main text.

used in 8 Å m/m video-recording. See Appendix D for details.

Fig. 8a shows that H_c decreases almost linearly with increase intergrain necking, the H_c of the particle with the intergrain necking degree, $p = 0$ is about 1,95 kOe, whilst when $p = 1$ it is about 1,30 kOe. Therefore, complete intergrain necking results in a decrease of about 0.65 kOe of H_c . It should be noted that this experimental trend is obtained for a particle with a fixed specific

surface area, grain size and aspect ratio, whereas the only variable morphological parameter is the intergrain necking degree.

Our theoretical model was applied to explain this experimental trend. Firstly, the introduction of an exchange interaction proportional to the intersphere contact area was necessary to reproduce the almost linear decrease of H_c with an increasing intergrain necking degree, p . Secondly, a scaling from the “theoretical p ” (this being the intersphere necking degree) to the “experimental p ” (this being the intergrain necking degree), was required due to the fact that the experimental p shown in Fig. 8a was estimated in a very simple way from the experimental data [Ref. 1 and also Appendix B][‡]. The results are shown in Fig. 8b. It is possible to see that the present model scheme agrees well with the experiment, if the value of the exchange anisotropy constant, K , can be assumed to be about 3.26 and the experimental p value is given by the theoretical p value multiplied by 5.3. This may be the first theoretical interpretation of the experimental dependence of H_c on the intergrain necking for very fine, acicular skeleton particles of α -Fe under the “chain-of-spheres” model in the symmetric fanning mode.

5. Preliminary study on grain size dependence of H_c

Another unsolved problem related to the very fine, highly acicular skeleton particles used in high-density magnetic recording media is “a dependence of H_c on the grain size”. In the case of α -Fe synthesized from goethite particles, it has been experimentally shown that H_c decreases with increasing grain size, see Fig. 9a [5].

It is well known that in the traditional Jacobs-Bean’s theory of the chain-of-spheres fanning mechanism there is no dependence of H_c on the particle size. Therefore, an extension of this theory is necessary such that it becomes applicable for explaining the previously mentioned experimental behavior. Here, we show the results of our preliminary study on this type of problem.

The idea is based on the possibility of grain size dependence of the parameter K , which represents the exchange anisotropy acting through the contact area. The value of K for the skeleton particle of α -Fe with the specific surface area of 50 m²/g and 160 Å of the grain size GS , was 3.26. We then tried to estimate, by applying multiregression analysis, the values of K for a skeleton particle of α -Fe with the specific surface area of 50 m²/g and a GS of 120, 140 and 200 Å, as partly shown in Fig. 10. The values of K thus estimated were found to be 4.34, 3.80 and 2.18,

[‡] In other words, the theoretical p value underestimates the realistic necking state, particularly with reference to the development of necking. The reason is as follows. The ISC with a finite number of spheres forms “one-sphere-chain” if the necking angle, η , tends to $\pi/2$, because the unit spheres, except two chain-end spheres, mathematically vanish. Then, the specific surface area of the ISC with (n, η) , $S(n, \eta)$ as defined in Appendix B overestimates the corresponding value of the real particle if η tends to $\pi/2$. Therefore, the contraction factor from the specific surface area of the unit sphere, S_0 to $S(n, \eta)$ overestimates the true value, which leads to an underestimation of the theoretical p . Therefore, the scaling from the theoretical p to the experimental p is required, if the theory developed here is to be applied to the experiments.

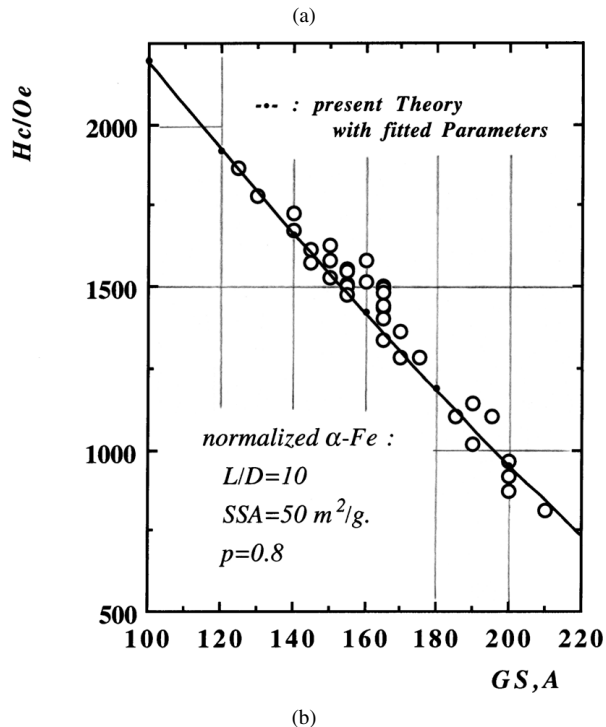
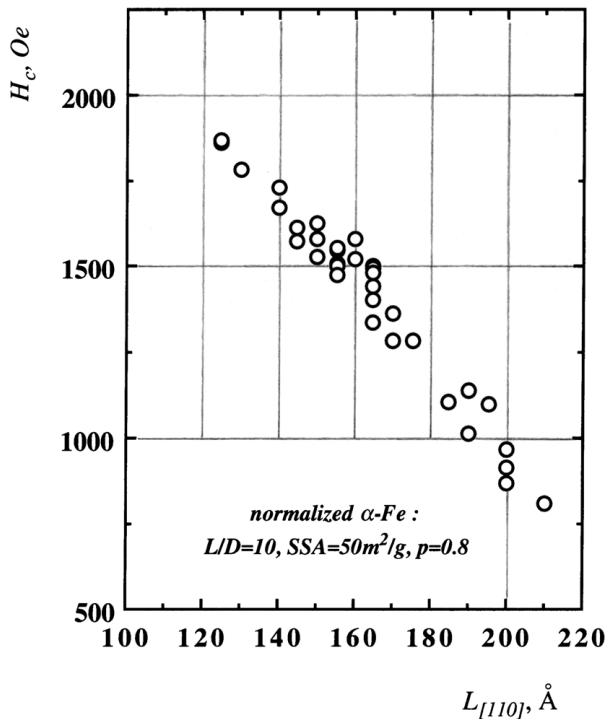


Figure 9 (a) The experimental dependence of H_c on crystallite size with respect to the [110]-plane, $L_{[110]}$, for very fine, highly acicular skeleton particles of α -Fe. (b) Interpretation by the present theory of the grain-size dependence of H_c for very fine, acicular skeleton-particles of α -Fe. Here, $L_{[110]}$ in Fig. 9a is replaced by GS in order to represent explicitly the grain size.

respectively. Therefore, the dependence of K on GS is almost “linear” in that $K(GS) = 7.57 - 2.70 \cdot GS$ ($\text{\AA}/100$), this empirical formula was used to interpret Fig. 9a. Furthermore, in Fig. 10, the experimental p is given by the theoretical p scaled by the data fitting parameter, $p(\text{exp}) = m \cdot p(\text{theor})$, where m is a scaling factor whose fitted formula is given by $14.9 - 6.00 \cdot GS$ ($\text{\AA}/100$).

Fig. 9b shows the result of our test where the predicted values of H_c as a function of GS for the skele-

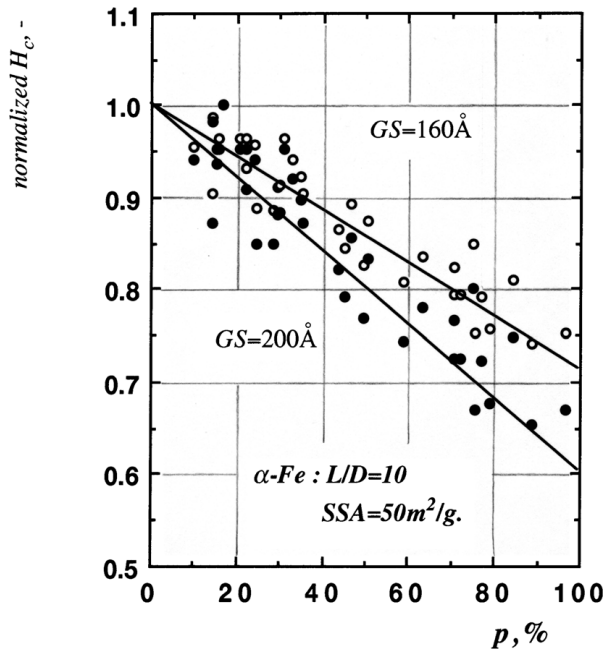


Figure 10 Normalized H_c with two typical morphological states plotted against p .

ton particles of α -Fe with a “normalized” morphology, $\{L/D = 10, p = 0.8, SSA = 50 \text{ m}^2/\text{g}\}$ were estimated according to then ormalized formula,

$$H_c \text{ in } \mu/a^3 = \alpha \cdot [1 - \exp\{-\beta((L/D) - 1)\}] \cdot \{1 + (a - b \cdot p) \cdot p\},$$

where $\alpha = 2.5231$, $\beta = 0.4652$; $a = 1.3742$ and $b = 1.5703$, as given in Appendix D, multiplied by the experimentally estimated values of H_c for the corresponding point-contacted state, which is given by the experimental value $p = 0$.

As is shown in Fig. 9b, the predicted values of H_c reproduce the experimental values of H_c as a function of GS . However, this does “not” mean that it is a “perfect” theoretical interpretation of the GS -dependence of H_c , as we had to assume an “unexpected” empirical GS -dependence on the “ad-hoc” parameter, m . Nevertheless, we believe that a dominant part of the physical origin of the grain-size dependence of H_c for fine acicular ferromagnetic skeleton particles is due to a grain size dependence on the exchange anisotropy parameter, K , which is acting between the grains.

6. Discussion

Only few experimental investigations on the fourth problem, that is to simulate the reversal of magnetization using our morphological model in order to determine how the particle morphology affects the reversal of the magnetization, have been carried out. Among them, Kaneko has reported on a study of the effect of annealing on H_c and its angular variation for alumite-nickel thin film media [18]. It was concluded that the increasing H_c due to annealing (from approx. 550–620 Oe as shown in Fig. 2 of ref. 19) can contribute to the parallel rotation mode instead of the symmetric fanning due to the increase in the contact area between adjacent grains in the skeketon particle morphology due

to the annealing process. Therefore, in following this conclusion, the intergrain necking apparently leads to an increasing H_c . However, the physical situation induced during the annealing process is very complicated. In general, annealing induces crystal growth that leads to an increasing sphere size and at the same time, the annihilation of the pores in the skeleton particle. The former results in a decreasing H_c , whilst the latter re-

sults in an increasing H_c [5]. Sometimes, interparticle sintering is also induced during annealing, this leads to the extremely large, decreasing H_c . This situation can be also found for the calcination temperature effect on H_c for fine, highly acicular skeleton particles of α -Fe (see, Table II). Here, the pore effect can be completely explained within the frame of the symmetric fanning mode of the “chain-of-spheres” model, if, the

TABLE II Data-base that was prepared to characterize the relationship between morphology and the reversal of magnetization for 8 m/m video-use acicular skeleton particles of α -Fe^a

Code	Surface ^(b) treatment	Cal. ^(c)		Red. ^(d) and property of α -Fe ^(e)						Memorandum
		T_c °C	SSA m ² /g	T_r °C	SSA m ² / g	GS Å	ρ g/cc	p %	H_c Oe	
-01	Si : 2.0 wt.%	400	117	375	68.2	160	5.18	19.3	1125	(*ml)
-02				400	56.8	175	5.40	35.1	1335	
-03				425	48.8	200	5.62	28.6	1240	
-04		500	105	375	66.1	155	5.34	29.4	1310	(*m2)
-05				400	55.9	170	5.46	45.1	1305	
-06				425	50.5	200	5.69	14.1	1225	
-07		600	78.7	375	60.2	150	5.47	58.9	1345	(*m2)
-08				400	55.4	165	5.59	49.5	1345	
-09				425	51.2	190	5.71	24.7	1290	
-10		650	76.2	375	58.5	145	5.53	72.7		(*ml)
-11				400	55.4	165	5.65	46.4	1470	
-12				425	49.3	165	5.51	84.3	1495	
-13		700	60.2	375	57.2	145	5.60	75.3	1390	
-14				400	46.6	160	5.72	96.4	1525	
-15				425	46.7	165	6.10	72.2	1540	
-16	Si : 3.0 wt.%	400	118	375	74.3	145	5.20	22.1	1225	
-17				400	65.2	165	5.06	30.9	1320	
-18				425	59.9	190	5.44	0.0	1360	(*m2)
-19				450	51.5	200	5.56	15.2	1285	(*m2)
-20		500	111	375	71.5	150	5.33	15.8	1310	
-21				400	64.7	155	5.45	29.7	1355	
-22				425	60.0	185	5.63	0.0	1340	(*m2)
-23				450	56.6	210	5.69	0.0	1305	(*m2)
-24		600	94.8	375	68.2	140	5.46	43.7	1340	
-25				400	61.9	165	5.58	16.7	1485	
-26				425	59.6	165	5.70	21.9	1485	
-27				450	47.7	195	5.82	32.6	1435	
-28		700	65.6	375	63.0	130	5.59	79.0	1405	
-29				400	55.2	150	5.71	70.7	1525	
-30				425	53.0	160	5.48	75.2	1520	
-31		750	48.1	425	46.1	170	5.89	76.9	1495	
-32	Si : 4.3 wt.%	500	114	425	65.1	160	5.56	11.6		(*ml)
-33				450	61.3	165	5.68	14.2	1475	
-34		700	71.8	375	63.1	125	5.58	88.8	1430	
-35				400	63.7	155	5.70	20.7	1480	
-36				425	53.9	155	5.82	63.2	1525	
-37		725	66.8	375	67.4	125	5.61	70.8	1405	
-38				400	62.8	155	5.98	9.9	1490	
-39				425	59.2	155	5.86	34.6	1535	
-40		750	61.3	375	57.9	120	5.65	115.2	1435	(*m3)
-41				400	63.0	140	5.77	50.6	1510	
-42				425	61.0	155	5.89	23.9	1545	

(^a): Powder of the goethite particle whose aspect ratio and specific surface area are 10 and 86.5 m²/g, respectively was used as a starting material.
(^b): Silica-hydroxide gel was coated on the particle surface of the goethite to prevent an interparticle sintering during hydrogen reduction process.
(^c): Calcination was carried out at T_c under a nitrogen atmosphere. SSA means a specific surface area of the calcinated material that is the powder of the modified goethite particle.
(^d): Reduction was carried out at T_r under a hydrogen atmosphere.
(^e): SSA, GS, ρ , p and H_c are morphological and magnetic parameters estimated for the reduced material:
SSA = specific surface area measured by the BET method that uses N₂ gas
GS = grain size with respect to {110} of BCC phase by the x-ray method
 ρ = particle density measured by a pycnometer
 p = intergrain necking degree calculated. For a detail, see the text.
 H_c = coercivity measured at packing degree of 10 vol.% under an external field of 10 kOe. A sample vibration magnetometer was used.
(*m1) : Reduction process was “poor” (:that means “not completely”).
(*m2) : Partly, abnormally-grown particles were found in the sample.
(*m3) : Partly, an interparticle sintering was found in the sample.

intraparticle pores can be treated as an intergrain misfitting [3]. Furthermore, the symmetric fanning mode remains preferentially in increasing the contact area between adjacent spheres in the chain-of-spheres, as shown in Fig. 5b. Therefore, Kaneko's conclusion, that the increasing H_c due to annealing contributes to the parallel rotation mode instead of the symmetric fanning mode, is a special case. Our interpretation of his investigation is that the annihilation of the intrapores is a possible physical factor resulting in the increasing H_c during annealing.

Sometimes theoretical investigations regarding the grain-size dependence of H_c for fine acicular particles are carried out, in relation to the thermal agitation phenomena of the magnetization [19]. As far as the author is aware, this dependence of H_c has not been theoretically investigated, except for the micromagnetics approach [20]. In our treatment, the definition of the effective exchange anisotropy constant, K , is not quantitative. K may be expressed in terms of $\sum J_i J_{i+1}$ and a geometrical factor depending on the contact area and the unit-sphere volume, where J_i is the spin of i -th sphere. In this instance, the value of K is dependent on sphere size. An exact estimation is now ongoing.

In trying to find a possible solution for the unsolved part of the fourth problem, it was possible to interpret the intergrain necking dependence of H_c of an acicular skeleton particle of α -Fe by extending Ishii-Sato's treatment in such a way as to include a type of exchange anisotropy. It was also found that the grain size dependence of H_c is derivable if this exchange anisotropy is dependent on the grain size. Although this dependence of the exchange anisotropy on the grain size is not yet fully investigated, the effects of the intergrain necking and the grain size on H_c are becoming a "well-defined" behavior. As far as the author is aware, this theoretical approach is the first of its kind in this field [10, 11].

In previous papers [6, 7], it has been shown that the angular variation of H_c is very strongly influenced by the presence of local aggregates such as a "bundle" or a "multiple". It was also found that the "apparently curling-like" angular variation of H_c can be realized by the presence of coexisting local aggregates where the "lateral" dipole-dipole interaction between the chain-of-spheres plays a dominant role in determining the magnetization reversal process. Therefore, based on the results obtained in the present study, it is most likely that the experimental behavior regarding the angular variation of H_c observed for the fine acicular skeleton particles with relatively high degrees of the intergrain necking [for examples, see our case [1] or another case reported by Bottoni *et al.* [21] will be due, in the main, to the coexistence of local aggregates.

7. Conclusions

Magnetization reversal of a long chain-of-spheres which are in contact with each other over a finite area was investigated in an effort to understand the quantitative effect of "intergrain necking" of fine, highly acicular ferromagnetic skeleton particles (particularly of α -Fe) consisting of the grains possible to treat as a single domain particle.

Based on Ishii-Sato's model of two interacting dipole spheres which are in contact with each other over a finite area, their treatment was directly extended to a long-sized chain, as increasing the intersphere contact area corresponds geometrically to an increase in the intergrain necking. Following this, a type of "exchange anisotropy" which is proportional to the contact area was introduced into the chain.

The symmetric fanning mode was preferential in increasing the intergrain necking and the introduction of anisotropy could provide a decreasing coercivity with increasing intergrain necking. This quantitatively reproduces experimentally observed behavior in very fine, highly acicular skeleton particles of α -Fe.

On the other hand, no essential change in the behavior of the angular variation of the coercivity was induced, even if exchange anisotropy was introduced into the chain. Therefore, as shown in [6, 7], one of the most important factors affecting the angular variation of the coercivity could be a lateral interaction between the chains by the means of two dimensional local aggregates such as a "multiple" which unavoidably exist in the realistic fine acicular particles system.

Finally, under the present scheme, it has been discussed as to how to interpret the experimental dependence of the coercivity on the grain size, where a possibility to introduce an influence of the unit-sphere size on the characteristic constant of the exchange anisotropy is suggested.

Appendix A: Extension of Ishii-Sato's formulation to the long chain

The formulation on the reversal of the magnetization for the single long-sized Ishii-Sato's chain (ISC), which consists of the dipole spheres of n , is briefly reviewed. In order to simplify the understanding of the problem, here the same units, and, as similar notations as possible to those given by Ishii and Sato are used.

Total energy density

It is convenient to represent the total energy density, ε_{tot} , of a single long-sized ISC under an external magnetic field, H_{ex} , as the sum of three parts:

$$\varepsilon_{\text{tot}} = \varepsilon_{\text{sphere}} + \varepsilon_{\text{intersphere}} + \varepsilon_{\text{ext}}. \quad (\text{A.1})$$

In the Cartesian co-ordinate system, without a loss of generality, it is possible to assume that the major axis of the ISC is located on the O - z axis and that the external field is applied in the direction of (θ_o, ϕ_o) in polar coordinates. Because of the geometrical symmetry of the ISC, it is also possible to assume an ϕ_o of zero, which means the external field is located on the (z, x) -plane, see Fig. 3 in the text. The value θ_o is the aligned or orientation angle of the ISC. If we assume the existence of a non-magnetic, thin layer on the surface of the unit sphere of which the ISC consists, these three terms can be formulated as follows.

On-sphere interaction term, $\varepsilon_{\text{sphere}}$

The first term on the right-hand side of Equation A.1, $\varepsilon_{\text{sphere}}$, represents the total self-energy of the dipole distributed on each sphere and is represented by the linear

combination:

$$\varepsilon_{\text{sphere}} = \sum_{i=1}^n \varepsilon_{\text{sphere}}(i). \quad (\text{A.2a})$$

Each sphere contribution, $\varepsilon_{\text{sphere}}(i)$ for $i = 1, 2, \dots, n$, can be given by:

$$\varepsilon_{\text{sphere}}(i) = C \cdot (\sin^2 \theta_i \cdot P_{s,i} + \cos^2 \theta_i \cdot Q_{s,i}), \quad (\text{A.2b})$$

where

$$C = M^2 \cdot r^3 / (\mu_o \cdot V), \quad (\text{A.2c})$$

$$P_{s,i} = (2^{1/2}/4) \int_{p_i}^{q_i} d\theta \int_{p_i}^{q_i} d\theta' (\sin \theta \cdot \sin \theta' / \beta_o^{1/2}) \cdot \{(\beta_o - \sin \theta \cdot \sin \theta') \cdot K(\alpha_o^{1/2}) - \beta_o \cdot E(\alpha_o^{1/2})\}, \quad (\text{A.2d})$$

and

$$Q_{s,i} = (1/2^{1/2}) \int_{p_i}^{q_i} d\theta \int_{p_i}^{q_i} d\theta' (\sin \theta \cdot \cos \theta \cdot \sin \theta' \cdot \cos \theta' / \beta_o^{1/2}) \cdot K(\alpha_o^{1/2}), \quad (\text{A.2e})$$

with

$$\alpha_o = \alpha(\eta = \pi/2) = 2 \sin \theta \cdot \sin \theta' / \beta_o,$$

which comes from the definition of $\alpha(\eta)$:

$$\alpha(\eta) = 2 \sin \theta \cdot \sin \theta' / \beta(\eta), \quad (\text{A.2f})$$

and

$$\beta_o = \beta(\eta = \pi/2) = 1 - \cos(\theta + \theta'),$$

which comes from the definition of $\beta(\eta)$:

$$\beta(\eta) = 1 - \cos(\theta + \theta') + 2(j-i) \cdot \cos \eta \times (\cos \theta - \cos \theta') + 2(j-i)^2 \cdot \cos^2 \eta. \quad (\text{A.2g})$$

Here, r is the sphere radius ($a/2$) and V is the total volume of the ISC under consideration. The lower and upper limits with respect to θ or θ' , p_i and q_i , of double integrations which appear in Equations A.2d and e are defined as:

$$p_i = 0 \quad \text{for } i = 0 \quad \text{and} \quad n, \\ = \eta \quad \text{for } i = 2, 3, \dots, n-1, \quad (\text{A.2h})$$

and

$$q_i = \pi - \eta \quad \text{for } i = 1, 2, \dots, n, \quad (\text{A.2i})$$

respectively.

K and E in Equations A.2d and e are the complete elliptic integral of the first and second kind respectively. Therefore, all $\{P_{s,i}\}$ and $\{Q_{s,i}\}$ for $i = 1, 2, \dots, n$ can be “numerically” estimated as a function of η (Appendix C). Here, $\{P_{s,i}\}$ and $\{Q_{s,i}\}$ for $i = 2, 3, \dots, n-1$ ($n \geq 3$) are interaction parameters of the new type which do not appear in the original Ishii-Sato’s treatment.

Inter-sphere interaction term, $\varepsilon_{\text{intersphere}}$

The second term on the right-hand side of Equation A.1, $\varepsilon_{\text{intersphere}}$, is the contribution from the dipole-dipole interaction among n -spheres and can be represented by

$$\varepsilon_{\text{intersphere}} = \sum_{i=1}^n \sum_{j=i+1}^n \varepsilon_{\text{intersphere}}(i, j). \quad (\text{A.3a})$$

The interaction term between i -th and j -th sphere, $\varepsilon_{\text{intersphere}}(i, j)$, is given by

$$\varepsilon_{\text{intersphere}}(i, j) = C \cdot \{\sin \theta_i \cdot \sin \theta_j \cdot \cos(\phi_i - \phi_j) \cdot P_{m,ij} + \cos \theta_i \cdot \cos \theta_j \cdot Q_{m,ij}\}, \quad (\text{A.3b})$$

where

$$P_{m,ij} = (1/2^{1/2}) \int_{r_i}^{S_i} d\theta \int_{r_j}^{S_j} d\theta' (\sin \theta \cdot \sin \theta' / \beta^{1/2}) \cdot \{(\beta - \sin \theta \cdot \sin \theta') \cdot K(\alpha^{1/2}) - \beta \cdot E(\alpha^{1/2})\}, \quad (\text{A.3c})$$

and

$$Q_{m,ij} = 2^{1/2} \int_{r_i}^{S_i} d\theta \int_{r_j}^{S_j} d\theta' \times (\sin \theta \cdot \cos \theta \cdot \sin \theta' \cdot \cos \theta' / \beta^{1/2}) \cdot K(\alpha^{1/2}), \quad (\text{A.3d})$$

Here, although the integrands which provide $\{P_{m,ij}\}$ and $\{Q_{m,ij}\}$ are apparently the same as those which give $\{P_{s,i}\}$ and $\{Q_{s,i}\}$, the lower and upper limits with respect to θ or θ' , r_i or r_j and s_i or s_j , of the double integrations which appear in Equations A.3c and d are defined as follows:

$$r_i = 0 \quad \text{for } i = 0, \\ = \eta \quad \text{for } i = 2, 3, \dots, n, \quad (\text{A.3e})$$

and

$$s_i = \pi - \eta \quad \text{for } i = 1, 2, \dots, n-1, \\ = \pi \quad \text{for } i = n, \quad (\text{A.3f})$$

respectively. Hence, we obtain a symmetry with $\{P_{m,ij}\}$ and $\{Q_{m,ij}\}$:

$$P_{m,ij} = P_{m,ji} \quad \text{and} \quad Q_{m,ij} = Q_{m,ji}. \quad (\text{A.3g})$$

All $\{P_{m,ij}\}$ and $\{Q_{m,ij}\}$ for $(i, j) = 1, 2, \dots, n$ can be “numerically” estimated as a function of η (Appendix C). Note again that in Equations A.3c and d, $\{P_{m,ij}\}$ and $\{Q_{m,ij}\}$ for $(i, j) = 1, 2, 3, \dots, n$ with $|i - j| \geq 2$ ($n \geq 3$) are interaction parameters of the new type which do not appear in Ishii-Sato’s treatment.

As is discussed in the text, the introduction of an exchange interaction into the ISC leads to, for example, from $P_{m,ij}$ to $P_{m,ij}^{\text{(eff)}}$ which is estimated by $P_{m,ij}$ multiplied by $(1 - K \cdot \sin^2 \eta)$, where K denotes the effective strength of the exchange interaction.

Interaction term with an external field, ε_{ext}

The third term on the right-hand side of Equation A.1, ε_{ext} , is represented by the linear summation over the interaction between the dipole on each sphere and an external field:

$$\varepsilon_{\text{ext}} = -M \cdot H_{\text{ex}} \sum_{i=1}^n v_i (\cos \theta_i \cdot \cos \theta_0 + \sin \theta_i \cdot \cos \phi_i \cdot \sin \theta_0), \quad (\text{A.4})$$

where v_i is the volume fraction of the i -th unit sphere to the total volume of the ISC. It is very easy and straightforward to confirm that Equations A.2–4 coincide completely with Ishii-Sato's treatment when n equals 2.

Reversal of magnetization

The path of the reversal of the magnetization, $(\theta(H_{\text{ex}}), \phi(H_{\text{ex}}))$, is determined by the well-known variational conditions:

$$\begin{aligned} \delta \varepsilon_{\text{tot}} / \delta \theta = 0, \quad \delta \varepsilon_{\text{tot}} / \delta \phi = 0 \quad \text{and} \\ (\delta^2 \varepsilon_{\text{tot}} / \delta \theta^2) \cdot (\delta^2 \varepsilon_{\text{tot}} / \delta \phi^2) = (\delta^2 \varepsilon_{\text{tot}} / \delta \theta \delta \phi)^2. \end{aligned} \quad (\text{A.5a})$$

under

$$\delta^2 \varepsilon_{\text{tot}} / \delta \theta^2 \geq 0 \quad \text{and} \quad \delta^2 \varepsilon_{\text{tot}} / \delta \phi^2 \geq 0. \quad (\text{A.5b})$$

The critical field of an irreversible rotation of magnetization, H_{cr} , can be directly estimated by (θ_t, ϕ_t) which satisfy critically Equations A.8a–e, as a function of $(\theta_0; n, \eta)$, as is shown in the following.

Symmetric fanning scheme

Our precise investigation regarding the relationship of dipole conformation with the reversal of the magnetization for a single snaked Jacobs-Bean's chain (snaked

JBC or SJBC, where a contact angle between two near-est neighbors of the unit spheres in the chain-of-spheres is introduced) has shown that the symmetric fanning in the sense of Jacobs-Bean is most reasonable if the contact angle is less than about 55° . In ISC, the symmetric fanning is defined as:

$$\theta_i = \theta \quad \text{and} \quad \phi_i = (-)^i \phi \quad \text{for } i = 1, 2, \dots, n, \quad (\text{A.6})$$

this leads to the simplified expressions of three terms of the total energy density:

$$\varepsilon_{\text{sphere}}(i) = C \cdot \{ \sin^2 \theta \cdot (P_{s,i} - Q_{s,i}) + Q_{s,i} \}, \quad (\text{A.7a})$$

$$\begin{aligned} \varepsilon_{\text{intersphere}}(i, j) = C \cdot \{ \sin^2 \theta \cdot (\cos \lambda_{ij} \phi \cdot P_{m,ij} - Q_{m,ij}) \\ + Q_{m,ij} \}, \end{aligned} \quad (\text{A.7b})$$

and

$$\begin{aligned} \varepsilon_{\text{ext}} = -M \cdot H_{\text{ex}} \sum_{i=1}^n v_i (\cos \theta \cdot \cos \theta_0 \\ + \sin \theta \cdot \cos \phi \cdot \sin \theta_0), \end{aligned} \quad (\text{A.7c})$$

where

$$\lambda_{ij} = (-)^{i-1} - (-)^{j-1}. \quad (\text{A.7d})$$

Therefore, Equations A.5a–e give rise to the following equations:

$$\begin{aligned} F_a = \sum_{i=1}^n (P_{s,i} - Q_{s,i}) \\ + \sum_{i=1}^n \sum_{j=i+1}^n [(\cos \lambda_{ij} \phi \cdot P_{m,ij} - Q_{m,ij}) \\ + (1/2) \lambda_{ij} \cdot \{ \sin \lambda_{ij} \phi / \sin \phi \} \cdot \{ (\tan \theta / \tan \theta_0) \\ - \cos \phi \} \cdot P_{m,ij}] = 0, \end{aligned} \quad (\text{A.8a})$$

TABLE A I Calculated morphological and characteristic parameters for ISC where $n = 10$: f_{i/l_0} , $(L/D)_{\text{eff}}^{*a}$, p , $P_s(i)$ and $Q_s(i)$

η , deg.	Morphological parameters			Characteristic parameters				Memo.
	f_{i/l_0}	$(L/D)_{\text{eff}}^{*a}$	p	i	$P_s(i)$	$Q_s(i)$		
0	1.0000	10	0	1	0.6894 8741	0.6908 3240		*b)
15	0.9693	9.6930	0.0972	1	0.6883 8484	0.6334 8011		*c)
				2	0.6878 1838	0.5743 5663		*d)
30	0.8794	8.7940	0.3325	1	0.6739 7925	0.5286 9677		*c)
				2	0.6651 0048	0.3411 7094		*d)
45	0.7364	7.6340	0.5922	1	0.6248 2358	0.4677 2636		*c)
				2	0.5849 5309	0.1388 4643		*d)
60	0.5500	5.5000	0.7826	1	0.5289 8793	0.4868 2866		*c)
				2	0.4247 2810	0.0319 2221		*d)
75	0.3329	3.3290	0.8202	1	0.3965 2358	0.5517 4243		*c)
				2	0.2032 9705	0.0020 7717		*d)
90	0.1000	1.0000	0	1	0.2549 7313	0.5889 4273		*c)
				2	0	0		*d)

*a: $(L/D)_{\text{eff}}$ is given by $n \cdot f_{i/l_0}$.

*b: Because of chain symmetry, $P_s(i) = P_s(1)$ and $Q_s(i) = Q_s(1)$ for $i = 2, 3, \dots, 10$.

*c: Because of chain-end symmetry, $P_s(10) = P_s(1)$ and $Q_s(10) = Q_s(1)$.

*d: Because of chain symmetry, $P_s(i) = P_s(1)$ and $Q_s(i) = Q_s(1)$ for $i = 3, 4, \dots, 9$.

$$(\mu_o/M) \cdot H_{cr} = -(R^3/V) \cdot (\sin\theta/\sin\theta_o) \\ \times \sum_{i=1}^n \sum_{j=i+1}^n \lambda_{ij} \cdot \{\sin\lambda_{ij}\phi/\sin\phi\} \cdot P_{m,ij}, \quad (\text{A.8b})$$

$$G_t = 2 \sum_{i=1}^n (P_{s,i} - Q_{s,i}) \cdot \cos 2\theta \\ + 2 \sum_{i=1}^n \sum_{j=i+1}^n (\cos \lambda_{ij}\phi \cdot P_{m,ij} - Q_{m,ij}) \cdot \cos 2\theta \\ + (V/R^3) \cdot (\mu_o/M) \cdot H_{ex} \cdot (\cos \theta \cdot \cos \theta_o \\ + \sin \theta \cdot \sin \theta_o \cdot \cos \phi) \geq 0, \quad (\text{A.8c})$$

$$H_t = \sum_{i=1}^n \sum_{j=i+1}^n \lambda_{ij}^2 \cos \lambda_{ij}\phi \cdot \sin^2 \theta \cdot P_{m,ij} \\ + (V/R^3) \cdot (\mu_o/M) \cdot H_{cr} \\ \cdot \sin \theta \cdot \sin \theta_o \cdot \cos \phi \leq 0, \quad (\text{A.8d})$$

and

$$F_b = G_t \cdot H_t + \left\{ \sum_{i=1}^n \sum_{j=i+1}^n \lambda_{ij} \cdot \sin(\lambda_{ij}\phi) \cdot \sin 2\theta \cdot P_{m,ij} \right. \\ \left. + (V/R^3) \cdot (\mu_o/M) \cdot H_{cr} \cdot \cos \theta \cdot \sin \theta_o \cdot \sin \phi \right\}^2 = 0. \quad (\text{A.8e})$$

Formally, for the ISC with a specified (n, η) , it is possible to use Equation A.8a to represent ϕ as a function of θ and θ_o : $\phi = \phi(\theta, \theta_o; n, \eta)$. Then, θ_B and ϕ_B which satisfy Equation A.8e can be derived as a function of θ_o :

$$\theta_B = \theta_B(\theta_o; n, \eta) \quad \text{and} \quad \phi_B = \phi_B(\theta_o; n, \eta), \quad (\text{A.8f})$$

respectively. Furthermore, the critical values, θ_m and ϕ_m , which critically, simultaneously satisfy Equations A.8c and d, are also derived as a function of θ_o :

$$\theta_m = \theta_m(\theta_o; n, \eta) \quad \text{and} \quad \phi_m = \phi_m(\theta_o; n, \eta), \quad (\text{A.8g})$$

If $\theta_o \leq \theta_m$, then the discontinuous transition point due to the irreversible rotation, θ_t and ϕ_t , is determined as minimum of $\{\theta_B$ or $\theta_m\}$, and its corresponding ϕ , respectively. If $\theta_o \leq \pi/4$, H_n and H_c are given from Equation A.8b by:

$$H_n = H_c = H_{cr}(\theta_t, \phi_t, \theta_o; n, \eta). \quad (\text{A.8h})$$

However, if $\theta_o > \pi/4$, then H_n is given by Equation A.8h, while H_c is essentially given by the coherent rotation. Furthermore, in the case of $\theta_o > \theta_m$, no symmetric fanning mode of the dipole conformation is possible for the reversal of the magnetization. It can be directly, but very tediously confirmed that Equations A.8a–e give exactly the same result as that of Ishii and Sato when n equals 2.

Parallel fanning scheme

The parallel fanning in the sense of Jacobs-Bean's scheme is very simply defined as:

$$\theta_i = \theta \quad \text{and} \quad \phi_i = 0 \quad \text{for } i = 1, 2, \dots, n. \quad (\text{A.9})$$

for the external field applied on (z, x) -plane.

Basically, in the SJBC, this incoherent irreversible rotation of the magnetization is not realized because of its higher energy state. However, it is instructive to check what parallel fanning does induce in the ISC. Using Equation A.9,

$$2 \tan(\theta_t + \theta_o) = \tan 2\theta_t, \quad (\text{A.10})$$

and

$$(\mu_o/M) \cdot H_{cr} = (\mu_o/M^2) \cdot K_u \cdot \sin 2\theta_t / \sin(\theta_t + \theta_o), \quad (\text{A.11})$$

where

$$(\mu_o/M^2) \cdot K_u = (R^3/V) \cdot \left\{ \sum_{i=1}^n (P_{s,i} - Q_{s,i}) \right. \\ \left. + \sum_{i=1}^n \sum_{j=i+1}^n (P_{m,ij} - Q_{m,ij}) \right\}, \quad (\text{A.12})$$

are very easily obtained from Equations A.5a and c. K_u as defined by Equation A.12 is a type of anisotropy constant in the parallel fanning. Equation A.10 means that the transition polar angle, θ_t , is only obtained as a function of θ_o .

In this mode of dipole conformation, H_n and H_c are given by

$$H_n = H_{cr},$$

and

$$H_c = H_{cr} \quad \text{for } \theta_o \leq \pi/4, \quad (\text{A.13a})$$

$$= H_{cr}(\theta_t = \pi/2 - \theta_o) \quad \text{for } \theta_o > \pi/4. \quad (\text{A.13b})$$

Again, it can be directly, but very tediously confirmed that Equations A.10–A.13 give completely the same result as that of Ishii and Sato when n equals 2.

Appendix B: Geometrical factors which characterize Ishii-Sato's chain

The specific surface area, S , of ISC with n unit-spheres whose radius, density and necking or sintering angles are r , ρ and η , respectively, are given by

$$S = (3/(\rho r)) \cdot \{1 + (n-1) \cdot \cos \eta\} / \\ \times \{1 + (n-1) \cdot \cos \eta \cdot (1 + \sin 2\eta/2)\}, \quad (\text{B.1})$$

which can easily be derived from the volume, V , and the surface area, S , which are expressed by following equations:

$$V = (4\pi r^3/3) \{1 + (n-1) \cdot \cos \eta \cdot (1 + \sin 2\eta/2)\}, \quad (\text{B.2})$$

TABLE A II Calculated morphological and characteristic parameters for ISC where $n = 10$: $P_m(i, j)$ and $Q_m(i, j)$

η , deg	i	j	$P_m(i, j)$	$Q_m(i, j)$	(i, j) providing the same value
0	2	1	0.1745 3943	-0.3497 0280	(3, 2), (4, 3), (5, 4), (6, 5), (7, 6), (8, 7), (9, 8), (10, 9)
	3	1	0.0218 1662	-0.0436 3323	(4, 2), (5, 3), (6, 4), (7, 5), (8, 6), (9, 7), (10, 8)
	4	1	0.0064 6418	-0.0129 2836	(5, 2), (6, 3), (7, 4), (8, 5), (9, 6), (10, 7)
	5	1	0.0027 2708	-0.0054 5415	(6, 2), (7, 3), (8, 4), (9, 5), (10, 6)
	6	1	0.0013 9626	-0.0027 9253	(7, 2), (8, 3), (9, 4), (10, 5)
	7	1	0.0008 0802	-0.0016 1605	(8, 2), (9, 3), (10, 4)
	8	1	0.0005 0884	-0.0010 1768	(9, 2), (10, 3)
	9	1	0.0003 4088	-0.0006 8177	(10, 2)
	10	1	0.0002 3941	-0.0004 7883	
	15	2	1	0.1912 5229	-0.2732 4901
3		1	0.0240 9825	-0.0355 1906	(10, 8)
		2	0.1912 0413	-0.2805 5187	(4, 3), (5, 4), (6, 5), (7, 6), (8, 7), (9, 8)
4		1	0.0071 4742	-0.0101 3635	(10, 7)
		2	0.0240 8771	-0.0381 9269	(5, 3), (6, 4), (7, 5), (8, 6), (9, 7)
5		1	0.0030 1636	-0.0040 5017	(10, 6)
		2	0.0071 4357	-0.0115 0765	(6, 3), (7, 4), (8, 5), (9, 6)
6		1	0.0015 4464	-0.0019 4828	(10, 5)
		2	0.0030 1454	-0.0048 8175	(7, 3), (8, 4), (9, 5)
7		1	0.0008 9397	-0.0010 5256	(10, 4)
	2	0.0015 4346	-0.0025 0572	(8, 3), (9, 4)	
8	1	0.0005 6300	-0.0006 1491	(10, 3)	
	2	0.0008 9337	-0.0014 5202	(9, 3)	
9	1	0.0003 7719	-0.0003 7955	(10, 2)	
	2	0.0005 6261	-0.0009 1513		
10	1	0.0002 6511	-0.0002 3852		
30	2	1	0.2289 1025	-0.1340 5640	(10, 9)
	3	1	0.0313 4579	-0.0164 0643	(10, 8)
		2	0.2280 1506	-0.1561 3263	(4, 3), (5, 4), (6, 5), (7, 6), (8, 7), (9, 8)
	4	1	0.0094 3084	-0.0034 8016	(10, 7)
		2	0.0311 4104	-0.0249 4233	(5, 3), (6, 4), (7, 5), (8, 6),
	5	1	0.0040 0012	-0.0007 0702	(10, 6)
		2	0.0093 5482	-0.0079 3710	(6, 3), (7, 4), (8, 5), (9, 6)
	6	1	0.0020 5346	0.0000 5818	(10, 5)
		2	0.0039 6403	-0.0034 3263	(7, 3), (8, 4), (9, 5)
	7	1	0.0011 9017	0.0002 8448	(10, 4)
	2	0.0020 3359	-0.0017 7767	(8, 3), (9, 4)	
8	1	0.0007 5024	0.0003 3957	(10, 3)	
	2	0.0011 7809	-0.0010 3511	(9, 3)	
9	1	0.0005 0294	0.0003 3590	(10, 2)	
	2	0.0007 4235	-0.0006 5427		
10	1	0.0003 5734	-0.0018 7662		
45	2	1	0.2586 5153	-0.0295 8398	(10, 9)
	3	1	0.0442 7180	0.0015 4355	(10, 8)
		2	0.2532 4050	-0.0589 0445	(4, 3), (5, 4), (6, 5), (7, 6), (8, 7), (9, 8)
	4	1	0.0141 0720	0.0029 1782	(10, 7)
		2	0.0428 8383	-0.0110 9211	(5, 3), (6, 4), (7, 5), (8, 6), (9, 7)
	5	1	0.0061 1586	0.0024 8574	(10, 6)
		2	0.0135 7108	-0.0038 9381	(6, 3), (7, 4), (8, 5), (9, 6)
	6	1	0.0031 7408	0.0019 5990	(10, 5)
		2	0.0058 5652	-0.0017 5904	(7, 3), (8, 4), (9, 5)
	7	1	0.0018 5149	0.0015 4393	(10, 4)
	2	0.0030 2977	-0.0009 3049	(8, 3), (9, 4)	
8	1	0.0011 7196	0.0012 3429	(10, 3)	
	2	0.0017 6316	-0.0005 4823	(9, 3)	
9	1	0.0007 8794	-0.0010 0397	(10, 2)	
	2	0.0011 1406	-0.0003 4902		
10	1	0.0005 8518	-0.0117 4451		
60	2	1	0.2490 1641	0.0080 6189	(10, 9)
	3	1	0.0619 3860	0.0079 5398	(10, 8)
		2	0.2293 6420	-0.0126 7261	(4, 3), (5, 4), (6, 5), (7, 6), (8, 7), (9, 8)
	4	1	0.0228 7095	0.0051 0371	(10, 7)
		2	0.0556 1399	-0.0025 4585	(5, 3), (6, 4), (7, 5), (8, 6), (9, 7)
	5	1	0.0105 9225	0.0034 8242	(10, 6)
		2	0.0201 8455	-0.0010 6375	(6, 3), (7, 4), (8, 5), (9, 6)
	6	1	0.0059 9326	0.0025 0768	(10, 5)
		2	0.0092 2869	-0.0005 2868	(7, 3), (8, 4), (9, 5)
	7	1	0.0033 9154	0.0018 8391	(10, 4)
	2	0.0049 1293	-0.0002 9485	(8, 3), (9, 4)	

(Continued).

TABLE A II (Continued).

η , deg	i	j	$P_m(i, j)$	$Q_m(i, j)$	(i, j) providing the same value	
75	8	1	0.0021 7660	0.0014 6353	(10, 3)	
		2	0.0029 0532	-0.0001 7924	(9, 3)	
	9	1	0.0014 7755	0.0011 6799	(10, 2)	
		2	0.0018 5390	-0.0001 1639		
	10	1	0.0012 4092	-0.0397 6300		
	75	2	1	0.1741 4403	0.0045 0639	(10, 9)
			3	0.0738 6431	0.0033 2638	(10, 8)
		4	2	0.1280 5312	-0.0008 2717	(4, 3), (5, 4), (6, 5), (7, 6), (8, 7), (9, 8)
			1	0.0374 5064	0.0023 4375	(10, 7)
		5	2	0.0516 3030	-0.0001 4813	(5, 3), (6, 4), (7, 5), (8, 6), (9, 7)
1			0.0209 8845	0.0017 1292	(10, 6)	
6		2	0.0254 7688	-0.0000 6956	(6, 3), (7, 4), (8, 5), (9, 6)	
		1	0.0127 0974	0.0012 9559	(10, 5)	
7		2	0.0139 6326	-0.0000 4080	(7, 3), (8, 4), (9, 5)	
		1	0.0081 8968	0.0010 0903	(10, 4)	
8	2	0.0082 9530	-0.0000 2611	(8, 3), (9, 4)		
	1	0.0055 4906	0.0008 0543	(10, 3)		
9	2	0.0052 5835	-0.0000 1758	(9, 3)		
	1	0.0039 1725	0.0006 5636	(10, 2)		
10	2	0.0035 1345	-0.0000 1229			
	1	0.0046 3344	-0.1104 4104			

and

$$S = 4\pi r^2 \{1 + (n - 1) \cdot \cos \eta\}. \quad (\text{B.3})$$

Because the corresponding specific surface area to the JBC, S_0 , is

$$S_0 = S(\eta = 0) = (3/\rho r), \quad (\text{B.4})$$

the contraction factor from S_0 to S as is defined in the text, f , is estimated by

$$f = S(\eta)/S_0 = \{1 + (n - 1) \cdot \cos \eta\} / \{1 + (n - 1) \cdot \cos \eta \cdot (1 + \sin 2\eta/2)\}, \quad (\text{B.5})$$

from which the necking factor, p is calculated as

$$p = 3(n/(n - 1)) \cdot (1 - f). \quad (\text{B.6})$$

An experimental method which estimates the values of p and η is as follows. Basically, because R can be experimentally evaluated from the grain size by the wide angle X-ray diffraction profile and/or from direct observation based on a transmission electron microscope (TEM) image, and ρ can be experimentally evaluated by a pycnometry, then it is possible to experimentally estimate S_0 from Equation B.4. Therefore, combined with an experimental S value, as evaluated for example by an N_2 adsorption method, it is possible to use Equation B.5 to estimate f . Then, p and η can be obtained from Equations B.6 and B.5 if n can be assumed to be the aspect ratio of the particle, this can be estimated from the TEM image.

Appendix C: Numerical values of $\{P_s, Q_s\}$ and $\{P_m, Q_m\}$ for Ishii-Sato's chain where $n = 10$

Table A.I shows the morphological parameters and $\{P_s, Q_s\}$ as a function of η , whereas $\{P_m, Q_m\}$ as a function of η is shown in Table A.II. $f_{1/10}$ in Table A.I

is a contraction factor from a JBC to ISC with respect to the axial length.

Appendix D: H_c as a function of the aspect ratio and intergrain necking

The calculations of H_n and H_c as a function of θ_0 and p were also carried out for the ISC where $n = 3, 4$ and 5 . As is partly indicated by Appendix C, changing the the number of the spheres and the necking angle simultaneously leads to a varying effective aspect ratio (that

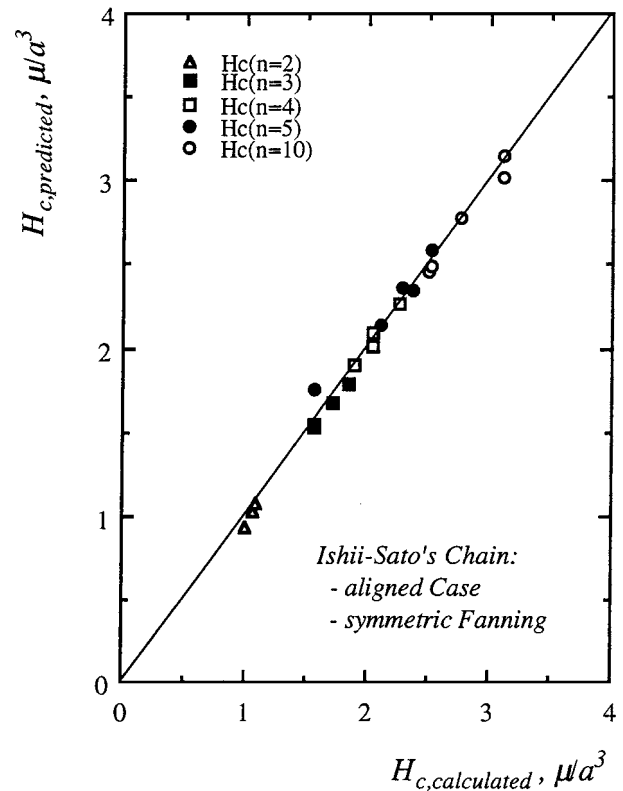


Figure A1 Comparison of the directly calculated values and the regression-based prediction of H_c for an ISC where $n = 2, 3, 4$ and 10 , in the symmetric fanning mode.

is defined as the effective length of the chain divided by the effective diameter) and necking factor. Therefore, in order to obtain the “pure” intersphere necking effect on the magnetization reversal, a regression analysis was necessary. As one of the results, the following formula was heuristically obtained having an accuracy of the multiple correlation coefficient of 99.4% for the dependence of H_c on the effective aspect ratio and the intersphere necking of the ISC aligned along the external field in the symmetric fanning mode:

$$H_c \text{ in } \mu/a^3 = \alpha \cdot [1 - \exp\{-\beta((L/D) - 1)\}] \cdot \{1 + (a - b \cdot p) \cdot p\},$$

where $\alpha = 2.5231$, $\beta = 0.4652$; $a = 1.3742$ and $b = 1.5703$.

Fig. A.I. demonstrates the accuracy of the above formula. By applying this regression formula, the pure effect of the intersphere necking on H_c for an ISC with normalized morphology as characterized by the effective aspect ratio, can be obtained.

References

1. T. TAGAWA, K. SUDOH, S. TAKAHASHI, M. MATSUNAGA and K. OHSHIMA, *IEEE Trans. Magn.* **MAG-21** (1985) 1492.

2. K. OHSHIMA, *ibid.* **MAG-22** (1986) 726.
3. *Idem.*, *ibid.* **MAG-23** (1987) 2826.
4. *Idem.*, *J. Magn. Magn. Mat.* **79** (1989) 276.
5. *Idem.*, *J. Asso. Mater. Eng. Resources* **3** (1990) 7 (Sozai-Busseigaku Zasshi, in Japanese).
6. *Idem.*, *J. Mat. Sci. Letters* **13** (1994) 361.
7. *Idem.*, *J. Mat. Sci.* **31** (1996) 519.
8. I. S. JACOBS and C. P. BEAN, *Phys. Rev.* **100** (1955) 1060.
9. Y. ISHII and M. SATO, *J. Appl. Phys.* **57**(2) (1985) 465.
10. *Idem.*, *ibid.* **59**(3) (1986) 880.
11. *Idem.*, *ibid.* **61**(1) (1987) 311.
12. K. OHSHIMA, *J. Mater. Res.* **13**(3) (1998) 711.
13. K. OHSHIMA, private communication with Prof. R. W. Chantrell of Keele University, UK (Jul. 1990).
14. E. H. FREI, S. SHTRIKMAN and D. TREVES, *Phys. Rev.* **106**(3) (1957) 446.
15. A. AHARONI and S. SHTRIKMAN, *ibid.* **109**(5) (1958) 1522.
16. A. AHARONI, *J. Appl. Phys.* **30**(4) (1959) 70S.
17. *Idem.*, “Application of Micromagnetics,” CRC Critical Reviews in Solid State Science (Aug. 1971) p. 121.
18. M. KANEKO, *IEEE Trans. Magn.* **MAG-17**(4) (1981) 1468.
19. A. LYBERATOS and R. W. CHANTRELL, *ibid.* **MAG-26**(5) (1990) 2119.
20. E. H. FREI, S. SHTRIKMAN and D. TREVES, *Phys. Rev.* **106**(3) (1957) 446.
21. G. BOTTONI, D. CANDOLFO, A. CECCHETTI, A. R. CORRADI and F. MASOLI, *JMMM* **104–107** (1992) 961.

Received 3 March 1999

and accepted 27 November 2000